AGU PUBLICATIONS

Geochemistry, Geophysics, Geosystems

RESEARCH LETTER

10.1002/2013GC005215

Key Points:
- A controlled oxygen fugacity thermal demagnetization apparatus was designed
- Alteration of metal-bearing rocks during heating is limited
- Paleointensity analyses of extraterrestrial rocks are possible

Supporting Information:
- Readme
- Data xls

Correspondence to:
C. Suavet,
csuavet@mit.edu

Citation:
Suavet, C., B. P. Weiss, and T. L. Grove (2014), Controlled-atmosphere thermal demagnetization and paleointensity analyses of extraterrestrial rocks, *Geochem. Geophys. Geosyst.*, *15*, 2733–2743, doi:10.1002/2013GC005215.

Received 23 DEC 2013
Accepted 25 JUN 2014
Accepted article online 1 JUL 2014
Published online 28 JUL 2014

Controlled-atmosphere thermal demagnetization and paleointensity analyses of extraterrestrial rocks

Clément Suavet[1], Benjamin P. Weiss[1], and Timothy L. Grove[1]

[1]Department of Earth, Atmospheric and Planetary Science, Massachusetts Institute of Technology, Cambridge, Massachusetts, USA

Abstract We describe a system for conducting thermal demagnetization of extraterrestrial rocks in a controlled atmosphere appropriate for a wide range of oxygen fugacities within the stability domain of iron. Thermal demagnetization and Thellier-Thellier paleointensity experiments on lunar basalt synthetic analogs show that the controlled atmosphere prevents oxidation of magnetic carriers. When combined with multidomain paleointensity techniques, this opens the possibility of highly accurate thermal demagnetization and paleointensity measurements on rocks from the Moon and asteroids.

1. Introduction

A central goal of extraterrestrial paleomagnetism is to measure the intensities of past planetary and nebular magnetic fields [*Weiss et al.*, 2010]. Records of these fields are provided by natural remanent magnetization (NRM) typically in the form of thermoremanence (TRM) acquired during cooling [*Nagata*, 1961; *Néel*, 1949]. TRM is best characterized using stepwise thermal demagnetization and remagnetization methods, because they reproduce the natural process of progressive magnetization thermal unblocking and blocking [*Tauxe*, 2010]. A major limitation to this methodology has been that most extraterrestrial rocks formed in environments which are orders of magnitude more reducing than at the Earth's surface (see Table 1 and *Wadhwa* [2008] for a review). As a result, heating such rocks in the Earth's atmosphere induces oxidation reactions that alter the magnetic carriers, demagnetizing them via recrystallization rather than thermal unblocking and also permanently changing their magnetic properties. Examples of thermal demagnetization and paleointensity experiments conducted in air that resulted in sample alteration include those of *Brecher and Leung* [1979], *Westphal and Whitechurch* [1983], *Westphal* [1986], and *Collinson* [1987] for ordinary chondrites and *Morden* [1992] for a eucrite.

As a result of these problems, extraterrestrial paleomagnetic studies have largely relied on alternating field (AF) methods in which the sample is demagnetized by a symmetric AC field of decreasing amplitude at room temperature. Paleointensities are obtained by comparing AF demagnetization of the NRM to that of a laboratory-induced anhysteretic remanent magnetization (ARM) or isothermal remanent magnetization (IRM) and relying on an empirically determined calibration factor [*Fuller and Cisowski*, 1987; *Gattacceca and Rochette*, 2004; *Kletetschka et al.*, 2004; *Yu*, 2010, 2006]. Although this method does not alter the magnetic carriers, it nevertheless has several key limitations. First, AF demagnetization unblocks NRM by grain coercivity rather than blocking temperature and therefore does not strictly reproduce the effect of thermal demagnetization. As a result, when NRM components overlap in bulk coercivity (due to, for example, a broad distribution of microcoercivities for grains with a narrow range of volumes), this can result in poorly isolated NRM components. Second, because of the relatively low peak AC fields ($<$ 300 mT) typically available in AF systems, the highest coercivity grains (i.e., $\sim$1 T for highly elongate single domain Fe grains) cannot be AF demagnetized. Third, AF methods typically achieve relatively uncertain paleointensity estimates because the calibration factor is different for every rock (varying typically by a factor of 3–5; Tikoo et al., 2014). If accuracy better than this is desired, then the sample has to be heated, thereby negating the key advantage of AF methods.

If sample alteration could somehow be mitigated during laboratory heating, the method of choice for determining the paleointensity of a TRM would be the Thellier-Thellier double heating method [*Thellier and*

Table 1. Oxygen Fugacities of Extraterrestrial and Terrestrial Rocks[a]

Rock Type	Oxygen Fugacity	Reference
Extraterrestrial		
Ordinary chondrites	IW-1	*Brett and Sato* [1984]
CV carbonaceous and Rumuruti-like chondrites	IW-1 to IW+5	*Righter and Neff* [2007]
CK carbonaceous chondrites	IW+7 to IW+9.5	*Righter and Neff* [2007]
Enstatite chondrites	IW-2	*Brett and Sato* [1984]
Aubrites	IW-2	*Brett and Sato* [1984]
Diogenites	IW-1	*Hewins and Ulmer* [1984]
Ureilites (nonchromite-bearing)	IW-3 to IW-2	*Goodrich et al.* [2013]
Ureilites (chromite-bearing)	IW+1	*Goodrich et al.* [2013]
Lunar basalts	IW-0.5 to IW-1	*Sato et al.* [1973]
Terrestrial		
Basalts	IW+3 to IW+5	*Ulmer and Woermann* [(2014)]
Granites	IW+5	*Zen* [1985]

[a]Note: following standard terminology, we express the oxygen fugacity relative to that of a given buffer in relative log units. To make the comparison easier, all fugacities are expressed relative to the IW buffer. For example, for 1 log(atm) below the iron-wüstite (IW) buffer, we write "IW-1."

Thellier, 1959] and its variants [*Aitken et al*., 1988; *Coe*, 1967; *Tauxe and Staudigel*, 2004; *Yu et al*., 2004]. In the Thellier-Thellier experiment, the sample is submitted to stepwise thermal demagnetization and remagnetization. Each temperature step is carried out in zero field and then one or more times in a known laboratory-applied field. The paleointensity is deduced from the ratio of the NRM lost and the partial TRM (pTRM) gained between two temperatures steps. Sample alteration can be monitored using repeated acquisitions of pTRM (pTRM checks).

There have been several previous attempts to eliminate alteration of extraterrestrial samples during thermal demagnetization. The most common method is to conduct the heating in vacuum [*Collinson et al*., 1973; *Dunn and Fuller*, 1972; *Fuller et al*., 1979; *Gose et al*., 1973; *Hoffman et al*., 1979; *Larson*, 1978; *Lawrence et al*., 2008]. The addition of a solid buffer, suggested by *Taylor* [1979] but never to our knowledge implemented, may improve the fugacity control. Sugiura and coauthors [*Sugiura and Strangway*, 1980, 1983; *Sugiura et al*., 1979] used a powdered Ti getter to capture the water from the samples before sealing the glass tube. However, all of these attempts gave largely unsatisfactory results, probably because typical laboratory vacuums (10^{-3}–10^{-5} torr) are still highly oxidizing (air at 10^{-5} torr has $fO_2 = 3 \times 10^{-9}$ atm, equivalent to IW+20 at 500°C).

Experiments were also conducted in pure Ar [*Chowdhary et al*., 1987] or in mixtures of H_2 diluted in N_2 [*Pearce et al*., 1976] or Ar [*Sugiura et al*., 1978]. The pure Ar experiments were unsuccessful because nominally inert gases actually contain impurities that render them highly oxidizing (even 99.999% pure gas can have fO_2 up to $\sim 10^{-6}$ atm when a minor amount of air is present as a contaminant, equivalent to IW +23 at 500°C). On the other hand, the experiments using mixtures of H_2 with either Ar or N_2 also failed, likely because they were too reducing. H_2, even diluted in an inert gas, creates an extremely reducing atmosphere because the only oxygen introduced into the system is as an impurity in the gases. For example, a mixture of 20% high-purity H_2 and 80% high-purity inert gas with typical levels of contaminants (5 ppm O_2, 5 ppm H_2O, 1 ppm CO_2, and 1 ppm CO) will have in $fO_2 < 10^{-35}$ atm at 500°C, equivalent to IW-7.

In summary, none of the above mentioned methods are satisfactory because they do not actually control the oxygen fugacity at a known value. Therefore, in hindsight, it is not surprising that essentially all extraterrestrial thermal demagnetization and Thellier-Thellier experiments have failed thus far to mitigate sample alteration. However, as long ago realized by the petrology community, controlled mixtures of oxidizing and reducing gases are expected to have far better buffering properties because the fO_2 is controlled by the balance of temperature-dependent reactions between the different gas species and varies with temperature [*Nafziger et al*., 1971]. The only magnetics experiments where such buffering gas mixtures were used were those of *Larson et al*. [1975], but no paleointensity analyses were performed with that apparatus.

Because gas mixtures equilibrate at temperatures as low as 300°C [*Burkhard and Ulmer*, 1995] and sample alteration is generally kinetically inhibited below these temperatures (as verified by our experiments below), they should be suitable for mitigating sample oxidation-reduction reactions during thermal demagnetization. Experiments in controlled reducing atmospheres have been successfully conducted with CO_2-H_2 mixtures for

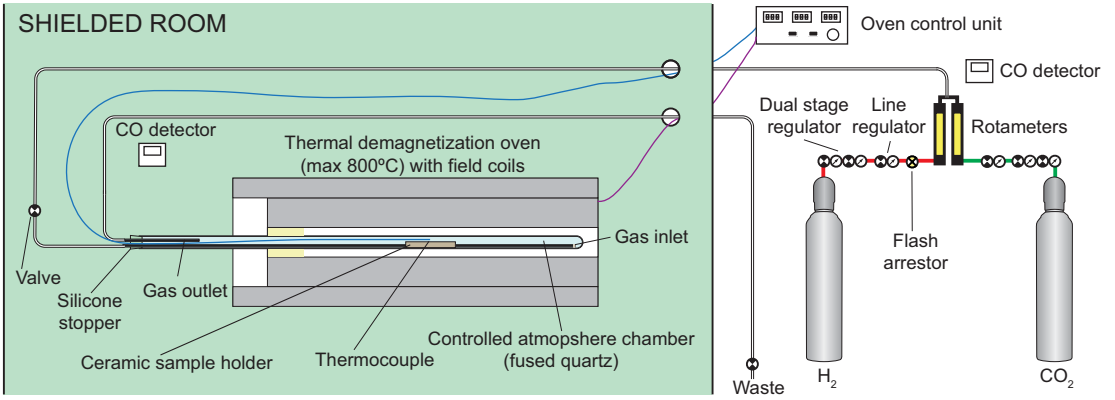

Figure 1. Controlled atmosphere thermal demagnetization apparatus. All the elements of the sample chamber are nonmagnetic.

both petrographic [e.g., *Sato*, 1971] and rock magnetic studies [*Bowles et al*., 2012] as well as with CO-CO_2 mixtures [*Huebner*, 1975]. Although both gas mixtures are effective at controlling fO_2, CO_2-H_2 mixing has the advantage of not employing a toxic gas (although H_2 is potentially explosive, the small gas fluxes typically used render it fairly safe for these applications).

Mixtures of H_2-CO_2 form O_2, H_2O, CO, and CH_4 by the following reactions [*Prunier and Hewitt*, 1981]:

$$CO_2 = CO + \tfrac{1}{2}\ O_2 \quad (1)$$

$$H_2 + \tfrac{1}{2}\ O_2 = H_2O \quad (2)$$

$$CO + 3H_2 = CH_4 + H_2O \quad (3)$$

In some conditions, graphite can precipitate, but this is only expected to happen for gas mixtures outside the stability domain of iron [*Prunier and Hewitt*, 1981]. By controlling the ratio of H_2 to CO_2, the oxygen fugacity at 800°C can be set in the range of 10^{-24}–10^{-10} atm (equivalent to ~IW-5 to IW+10; assuming that the mixing ratio can be controlled with a precision of 0.1%) [*Prunier and Hewitt*, 1981], which encompasses essentially the entire range of conditions in which known planetary samples formed (Table 1). With this goal, we designed what is to our knowledge the first thermal demagnetization and paleointensity apparatus that incorporates accurate fO_2 atmosphere and magnetic field control into a magnetically shielded environment.

We note that oxidation of metal grains is not the only process that can prevent paleointensity determination for extraterrestrial rocks. For rocks that contain Fe-Ni metal with Ni > ~5%, equilibrium and disequilibrium mineralogical transformations such as martensitic transformations and recrystallization to Widmanstätten and plessite intergrowths occur below the Curie point [*Cacciamani et al*., 2006; *Garrick-Bethell and Weiss*, 2010]. These can impart phase-transformation crystallization remanent magnetizations that render Thellier-Thellier experiments inapplicable. The presence of sulfides may also complicate paleointensity experiments: when the sulfur fugacity is not controlled, new metal grains can form by reduction of sulfides [*Keller et al*., 2010; *Larson*, 1978; *Watson et al*., 1974]. Therefore, the use of this method should provide the most benefit for kamacite-bearing rocks with low sulfide content.

In section 2, we describe the experimental setup of our controlled atmosphere apparatus and the calibration experiments. We then present in section 3 its application to the thermal demagnetization and paleointensity analyses of synthetic lunar basalts.

2. Experimental Setup

The controlled atmosphere apparatus (Figure 1) is a 33 mm outer diameter fused quartz tube inserted into an ASC Scientific TS-48SC thermal demagnetization oven situated in the MIT Paleomagnetism Laboratory magnetically shielded room. The maximum temperature that can be reached with this setup is ~800°C and the

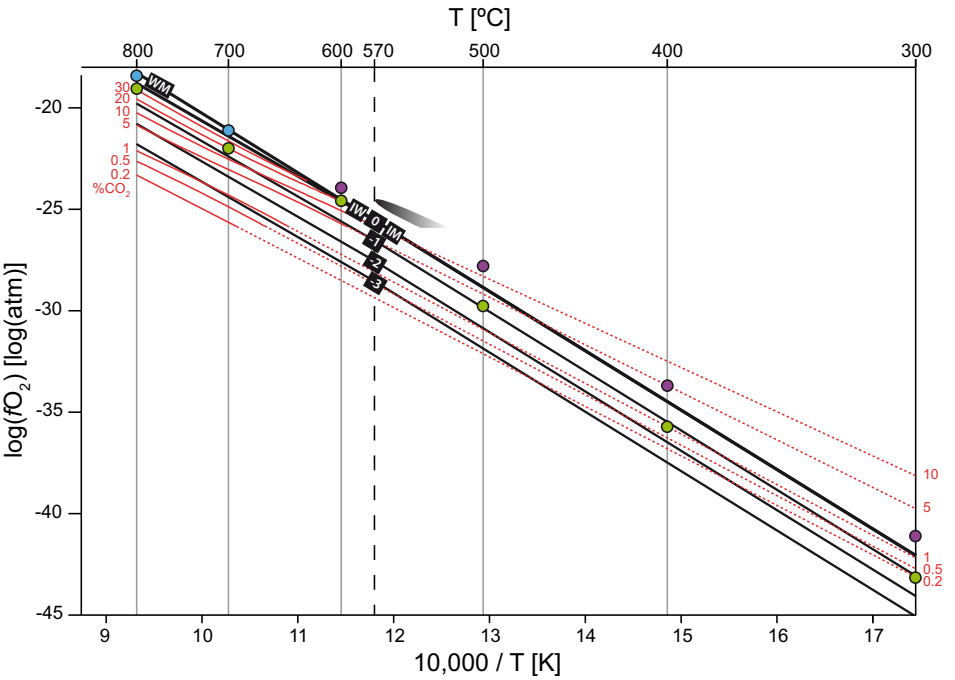

Figure 2. Calibration of the gas mixtures in our controlled-atmosphere thermal demagnetization apparatus. Shown is the inferred oxygen fugacity, log(fO_2), as a function of inverse temperature, 1/*T*. Black thick lines labeled "0" are iron-wüstite (IW) and iron-magnetite (IM) solid buffer curves from *Eugster and Wones* [1962] (based on measurements for IW, and theoretical calculations for IM), which intersect at ~570°C. Above this temperature, the IM curve splits into IW+0 and a wüstite-magnetite (WM) curves. Additional black solid lines represent −1, −2, and −3 log (atm) below the IW/IM buffer. Red solid lines represent calculated fugacities from *Prunier and Hewitt* [1981] for H_2-CO_2 gas mixtures of different compositions (in vol % CO_2), and dashed lines are low-temperature linear extrapolations. The dark shaded area encompasses the conditions in which graphite can precipitate [*Prunier and Hewitt*, 1981]. Green circles represent our experiments for which we observed iron was stable, blue circles represent experiments for which we observed that iron was oxidized to wüstite, and purple circles represent experiments for which we observed that iron was oxidized to magnetite. The fugacity for each of these experiments was calculated based on the controlled H_2-CO_2 gas mixture composition.

field measured inside the oven is typically < 20 nT. Samples are placed on a removable ceramic holder attached to a 6 mm outer diameter gas inlet quartz tube with ceramic paste. A platinum wire acting as a catalyst [*Burkhard and Ulmer*, 1995] is wrapped around the opening of the gas inlet. Once the peak temperature is reached in the oven, the temperature gradient along the sample holder is <5°C. The quartz tube is sealed with a silicone stopper. The gas mixture composition is controlled from outside the shielded room by adjusting the flow rates of H_2 and CO_2 with two rotameters. The range of possible flow rates is 0.01–2.28 × 10^{-6} m^3/s for CO_2 and 0.58–5.88 × 10^{-6} m^3/s for H_2. CO detectors are used to monitor potential H_2 leaks, but these are not expected to be problematic because of the small H_2 flow rates (the total flow is ~6 × 10^{-6} m^3/s during filling).

3. Calibration

To calibrate and test our system, we heated iron metal fragments (guaranteed 99.99% Fe by the producer) in gas mixtures of different compositions to temperatures between 300 and 800°C (Figure 2). At temperatures below ~570°C, iron oxidizes to form magnetite when the atmosphere is too oxidizing. Above ~570°C, iron oxidizes to form wüstite, which then further oxidizes to magnetite. The fO_2 conditions at which these reactions occur are given by the equations of *Eugster and Wones* [1962], which define the IW, IM, and wüsite-magnetite (WM) buffers. We calculated the proportions of H_2 and CO_2 required to reach fO_2 levels above and below the IW and IM buffers at different temperatures based on the tables of *Prunier and Hewitt* [1981] for log(fO_2) > −25.8 log(atm) and with linear extrapolation for more reducing conditions. For each of our heating experiments, the mixture corresponding to the target fO_2 at the temperature peak was introduced at room temperature and the system was sealed before heating. The expansion of the gas mixture with heating was accommodated by the elastic tubing on the inlet and waste sides of the chamber, resulting in a negligible increase of pressure. The system was kept at the target temperature for >30 min.

Table 2. Gas Mixtures (vol % CO_2) Required to Set the Fugacity at Various Levels Relative to the IM/IW Buffers

T (°C)	IM/IW	IM/IW-1	IM/IW-2	IM/IW-3
<300	1	0.2	0.2	0.2
300	1	0.2	0.2	0.2
350	2	0.5	0.2	0.2
400	3	1	0.5	0.2
450	5	2	0.7	0.2
500	7	3	1	0.2
550	10	4	1	0.5
600	20	5	2	0.5
650	30	10	3	0.7
700	35	10	4	1
750	40	15	5	1
800	40	15	5	1

Oxidation of iron to magnetite or to wüstite (visible as a change of color for a wüstite test sample from silver/gray to dark gray or bluish dark gray, respectively) conformed to the predictions using linear extrapolation of gas mixture fO_2 and buffer equations and consistent with the results of *Burkhard and Ulmer* [1995].

Because we sealed the system before heating and gas mixtures are more oxidizing relative to IW/IM buffer curves at low temperatures, it is possible that the gas mixtures may be too oxidizing as the temperature is rising. To determine whether this effect is significant, we conducted experiments with continuous flow of variable gas mixtures. Because we did not observe any differences in the stability of iron between the continuous flow and sealed experiments, we conclude that the heating is sufficiently rapid that redox reactions are quenched.

Table 2 presents the proportions of gases required to adjust the fO_2 at 0, 1, 2, or 3 log units below the IW and IM buffers [*Prunier and Hewitt*, 1981]. Since the most reducing mixture permitted by our setup is 0.2% CO_2 – 99.8% H_2 (limited by our ability to monitor small flow rates of CO_2), corresponding to a fO_2 of $\sim 10^{-43}$ atm at 300°C, it is not possible to set the fugacity below IM-1 log (atm) at this temperature. However, this value is still in the stability domain of iron.

4. Lunar Basalt Analogs

4.1. Thermal Demagnetization

To further test our system, we conducted thermal demagnetization experiments on lunar basalt analogs synthesized by *Grove and Beaty* [1980]. These samples were originally created to constrain the cooling rates of the Apollo samples and therefore have similar bulk compositions, cooling rates, and grain sizes resembling typical lunar basalts. Like Apollo 11 and 17 basalts, they contain essentially pure Fe metallic iron (Figures 3b, 3e, and 3h) with a Curie temperature of 780°C. However, the basalt analogs differ from Apollo basalts in not containing troilite, which allows us to separate the effects of metal oxidation and reduction from magnetostatic interactions between metal and troilite that are hypothesized to complicate analyses of the natural samples [*Chowdhary et al*., 1987]. We used samples of run numbers 18 (cooling rate 1.46°C/h), 45 (cooling rate 120°C/h), and 46 (cooling rate 62.7°C/h) from *Grove and Beaty* [1980] (hereafter named An-18, An-45, and An-46). These samples were synthesized in evacuated silica glass tubes in high-purity iron capsules with log(fO_2) near IW-1. An-18 contains glass, ilmenite, clinopyroxene, plagioclase, and silica, while An-45 and An-46 contain glass, olivine, ilmenite, and clinopyroxene. The samples are slabs of approximate dimensions 1 × 3 × 5 mm. Our petrographic observations suggest they are dominantly in the multidomain state, which is confirmed by hysteresis measurements: $M_{rs}/M_s = 10^{-2}$ and $H_{cr}/H_c = 13.5$ for saturation magnetization M_s, saturation remanent magnetization M_{rs}, coercive force H_c, and remanent coercive force H_{cr} [*Day et al*., 1977] (Figure 4). The metal grain sizes are in the range of 0.5–50 μm for An-18, 0.5–15 μm for An-45, and 0.5–15 μm for An-46. Their magnetic anisotropy degree P was determined to be ~1.01 by measuring their saturation magnetization (acquired imparted with a 2.5 T field pulse) along orthogonal directions.

We imparted a total TRM on all three samples by heating them to 800°C in a H_2-CO_2 mixture with log(fO_2) ~ IW-1 and cooling in a 100 μT field. For all experiments, the heating time was 15–30 min, the samples were kept at the peak temperature for 10–20 min, and the cooling time was ~20 min. An-45 was then thermally demagnetized in air (i.e., the demagnetization apparatus was used with the gas mixture replaced by air), while An-46 was demagnetized in the controlled atmosphere (IW-1; see Figure 5 and supporting information for the data). Up to ~300°C, both samples showed similar behavior, with a decay <10% and stable magnetization directions. Between 300 and 500°C, the magnetization of An-45 strongly decayed to ~20% of the initial moment while the magnetization direction was still stable. By comparison, An-46 only lost a few percent of its magnetization between these temperatures. Above 500°C, the magnetization of An-45 became directionally

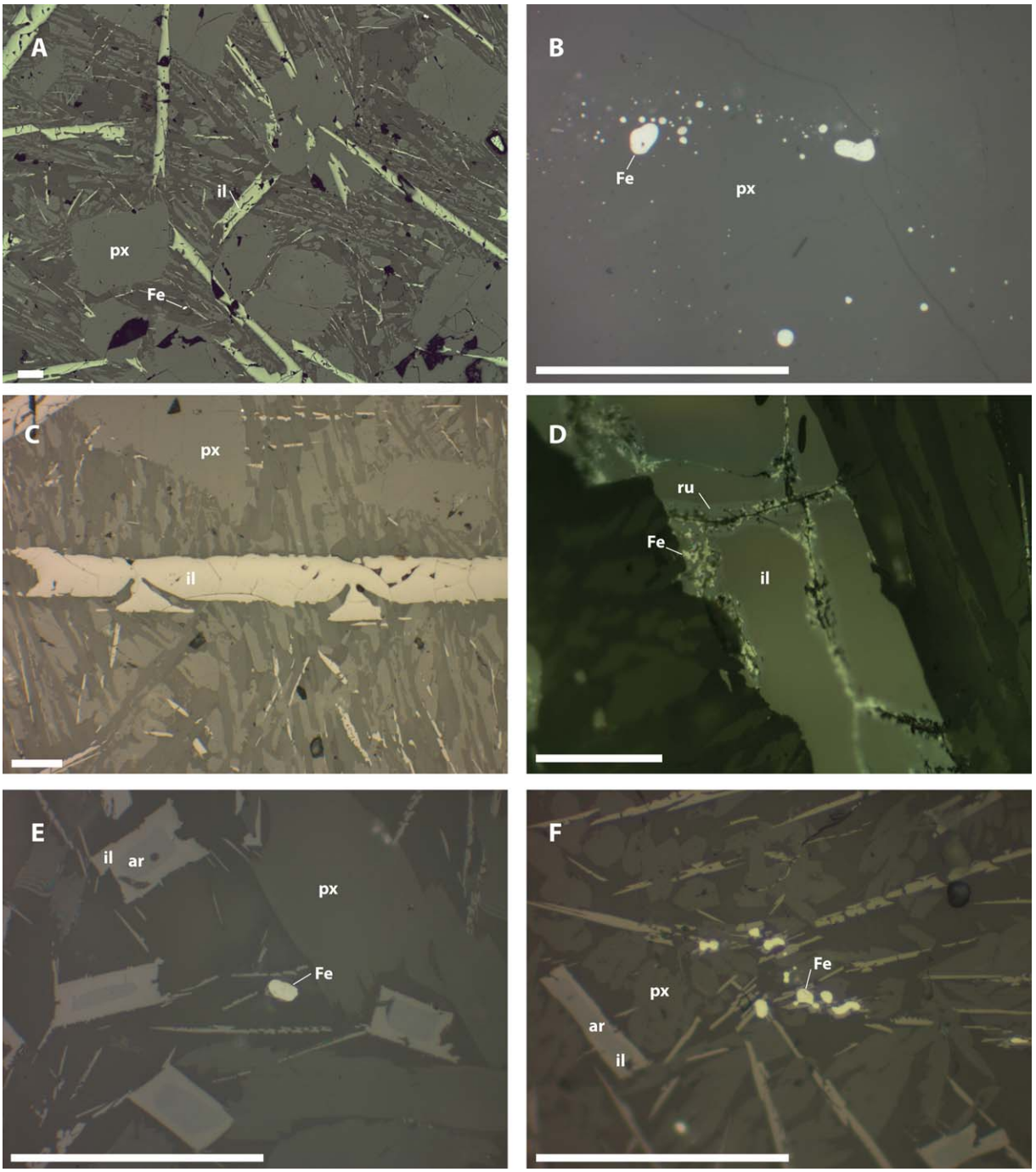

Figure 3. Optical reflected microscope images of synthetic lunar basalt samples. (a) An-18, showing ilmenite, pyroxene, and iron. (b) An-18, showing metal grains. (c) An-18, showing ilmenite. (d) An-18 after thermal demagnetization in controlled atmosphere to 800°C. New iron blebs in rutile were formed by reduction of ilmenite. (e) An-45, showing ilmenite with armalcolite cores, pyroxene, and iron. (f) An-45 after thermal demagnetization in air to 800°C; iron grains do not appear to be altered. px = pyroxene, il = ilmenite, ar = armalcolite, Fe = iron, ru = rutile. The scale bars are 100 μm.

unstable and rapidly decayed with a concave up demagnetization shape to the demagnetization curve. An-46 showed a moderate decay below 700°C and remarkable directional stability; most of the intensity decay occurred between 750 and 775°C and with a concave down demagnetization curve.

The magnetization decay of An-45 at moderate temperature was clearly attributable to alteration. The metallic iron was probably oxidized to magnetite as indicated by the peak temperature of demagnetization (which was near the Curie point of magnetite) and the destruction of its magnetic record. However, most

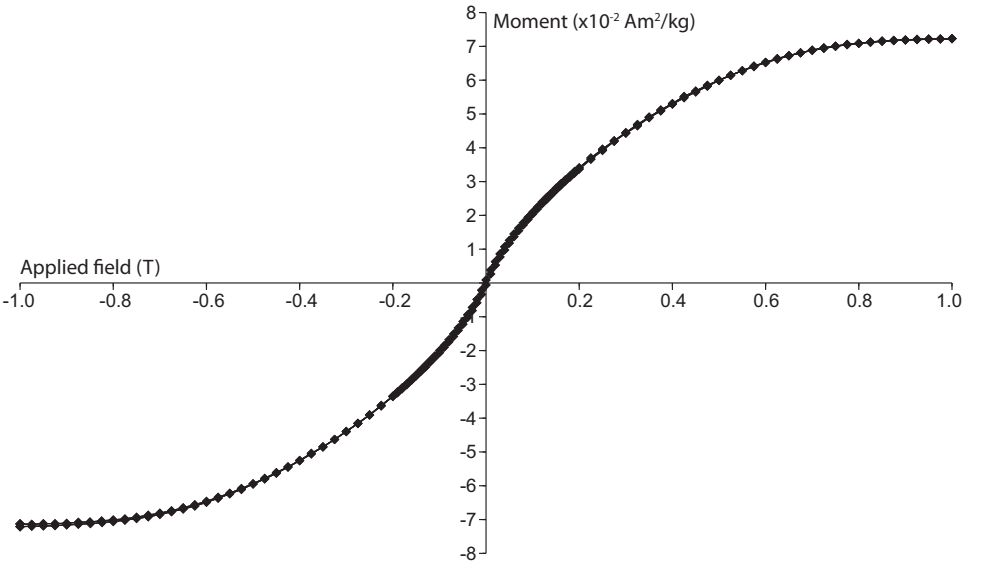

Figure 4. Room temperature hysteresis loop after subtracting paramagnetic and diamagnetic contributions for An-46.

iron grains appear unaltered in reflection microscopy (Figure 3f), and microprobe analyses do not show detectable amounts of oxides. Oxidation may be limited to the surface of the large metal grains and to efficiently magnetized smaller grains. Regardless, it is nevertheless sufficient to drastically alter the magnetic record. For An-46, the continuous decay to 775°C, as well as the concave down shape of the demagnetization curve [*Dunlop and Özdemir*, 1997], are both consistent with thermal demagnetization by unblocking of metallic Fe grains. We measured the saturation magnetization—imparted by a 2.5 T field pulse—of two fragments of An-18 and An-45 before and after heating to 400°C in air and in the gas mixture, respectively. The magnetization of the fragment heated in air increased by 64% after heating, whereas that of the fragment heated in the gas mixture increased by 9%. Therefore, the controlled atmosphere apparatus makes it possible to study the TRM of metal-bearing samples. In particular, the success of our experiments demonstrates that although the gas reactions that maintain an equilibrium oxygen fugacity may be inhibited below ~300C°C, alteration of the solid sample is also kinetically inhibited at these temperatures, making controlled oxygen fugacity thermal demagnetization feasible.

4.2. Paleointensity Experiment

We conducted a Thellier-Thellier paleointensity experiment on the total TRM imparted to sample An-18 using the Coe protocol [*Coe*, 1967] (Figure 6). For each temperature step, the sample was heated once in zero field and once in a 100 μT laboratory field for pTRM acquisition (see supporting information for the list of steps and the data). Checks for alteration, in which pTRM was acquired at selected lower temperatures, were made after heating to 600°C (pTRM checks at 400 and 500°C), 700°C (pTRM check at 600°C), 750°C (pTRM check at 700°C), and 770°C (pTRM check at 750°C).

The NRM direction was very directionally stable throughout the demagnetization, as indicated by the maximum angular deviation (MAD = 8.1°) from a least squares fit [*Kirschvink*, 1980], and was origin trending as indicated by the fact that its deviation angle (DANG) of 4.1° [*Tauxe and Staudigel*, 2004] is less than the MAD (see Table 3). Typical for multidomain grains, the curve is concave-up, which would lead to an overestimation of the paleointensity in the low-temperature segment [*Levi*, 1977] without additional mitigating experiments [i.e., *Wang and Kent*, 2013]. Note that this feature is inherent to multidomain magnetic grains and does not result from sample alteration. In particular, as demonstrated by the reproducibility of the pTRM checks, alteration is negligible up to 750°C. The difference ratio sum (DRATS) alteration parameter [*Shaar and Tauxe*, 2013; *Tauxe and Staudigel*, 2004] in the temperature range 20–750°C is ~20% (see Table 3), below the cutoff value of 25% above which paleointensity experiments are typically deemed unacceptable. However, the total TRM acquired at the last step of the experiment (770°C) shows a 150% increase in moment compared with the initial acquisition. This indicates that new magnetic grains were formed. In

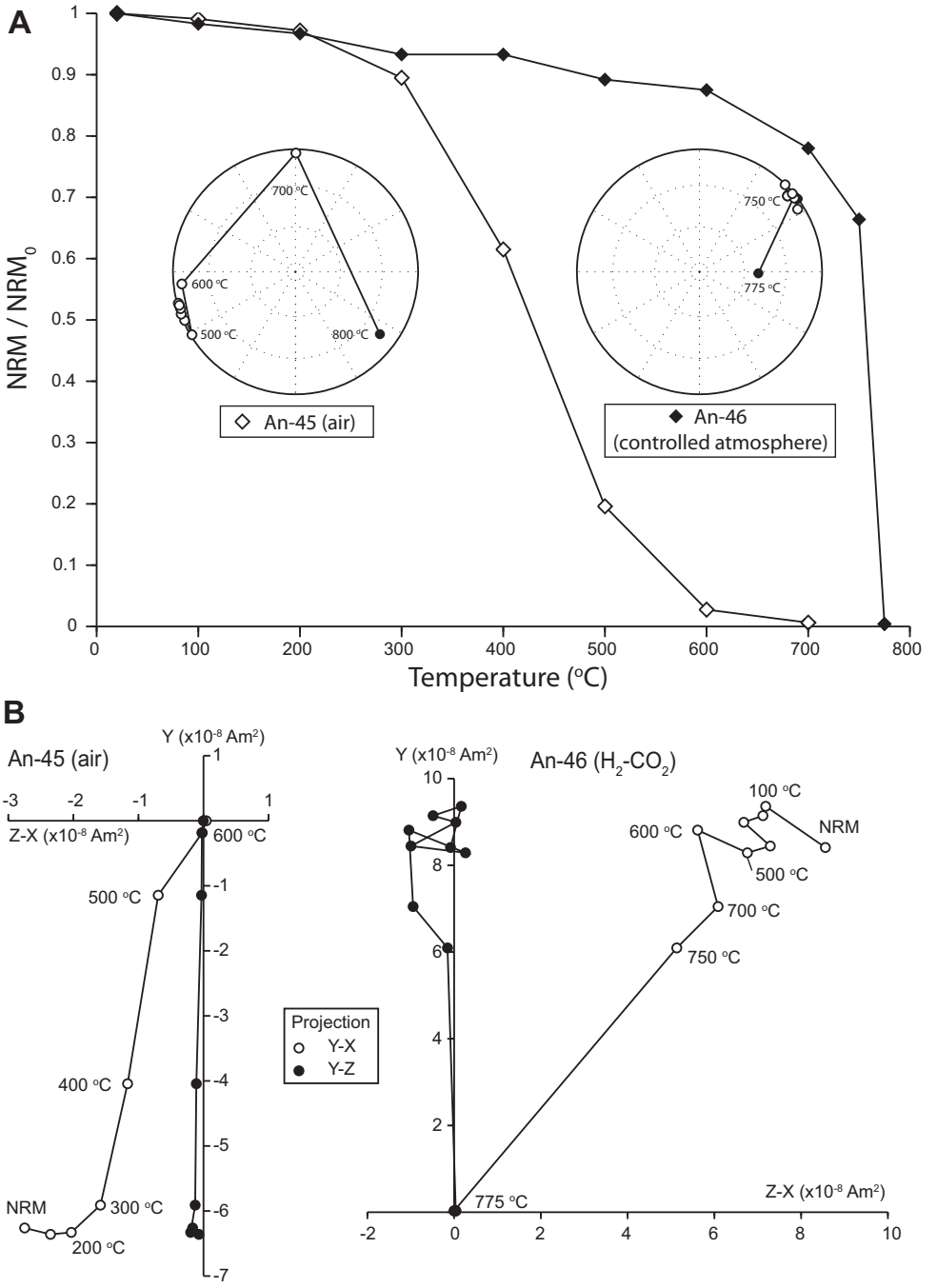

Figure 5. Thermal demagnetization of lunar basalt analogs in air and a controlled atmosphere. (a) Direction and intensity of magnetization normalized to the total TRM throughout the demagnetization. Insets show equal area plots of the magnetization direction, with closed and open symbols representing lower and upper hemispheres, respectively. (b) Two-dimensional projection of the NRM vectors of An-45 and An-46. Solid (open) circles represent end points of magnetization projected onto the y-z (y-x) planes.

particular, our electron microscopy data show that new iron was produced by reduction of ilmenite to rutile plus metal (Figure 3d) [see also *Pearce et al.*, 1976]. As the oxygen fugacity in which the samples were synthesized was controlled by a different method (evacuated silica glass tubes) and at much higher temperatures than in our experiment, it cannot be excluded that some minerals are unstable in our gas mixture. *Taylor et al.* [1972] determined the fugacity at which ilmenite reduction occurs for temperatures above 850°C. Extrapolation of their results predict a $\log(fO_2) \sim -19$ at 800°C, or ~IW-0.5. It may be possible to avoid reduction of ilmenite by using more oxidizing gas mixtures at high temperature. However, alteration of magnetic carriers is

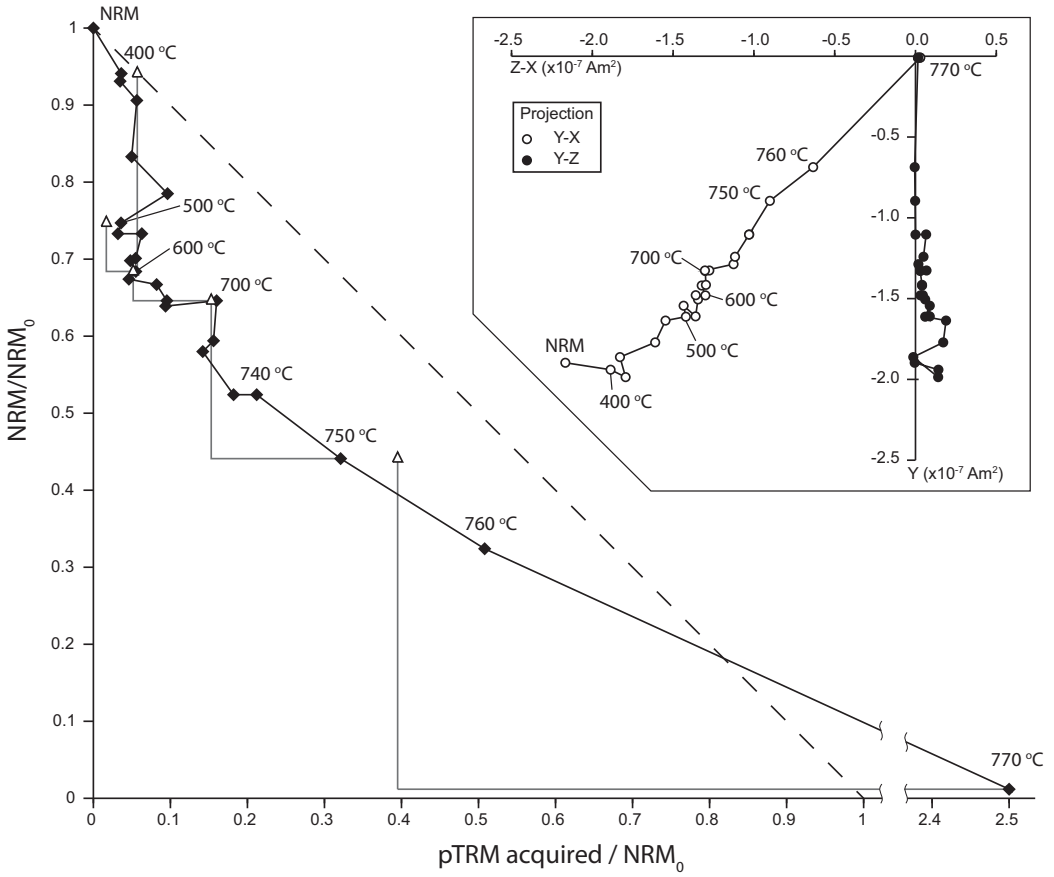

Figure 6. Paleointensity experiment on lunar basalt analog sample An-18. Shown is the NRM lost (normalized to initial NRM, NRM_0) as a function of pTRM gained (normalized to NRM_0). Triangles are pTRM checks. The dashed line represents ideal behavior expected for single domain grains without alteration. The inset shows the orthographic projection of the NRM for zero-field steps. Solid (open) circles represent end points of magnetization projected onto the y-z (y-x) planes.

extremely limited up to at least 750°C, which should be sufficient to obtain reliable paleointensity estimates for extraterrestrial rocks.

Note that the lunar basalts on which the analogs are based have cooling times from the Curie temperature to the lunar surface temperature of the order of 10^2-10^3 days. The cooling times in our experiments are orders of magnitude shorter. However, since we used the same fast cooling rate to impart the TRM as that used for our paleointensity experiments, we do not need to make a cooling rate correction [*Halgedahl et al.*, 1980] to our paleointensities.

We also note that since the initial TRM was imparted by heating the samples in the gas mixture and reduction of ilmenite occurs at high (>750°C) temperature, part of the original TRM must have been carried by iron grains produced from ilmenite. The demagnetization of An-46 shows that these grains have unblocking

Table 3. Statistics for An-18 NRM Direction[a]

Parameter	Temperature Range	Value	Reference
NRM		(221.0°,−0.1°)	
Fit	20–770°C	(224.8°,2.3°)	
MAD	20–770°C	8.1°	*Kirschvink* [1980]
DANG	20–770°C	4.1°	*Tauxe and Staudigel* [2004]
DRATS	20–750°C	20%	*Tauxe and Staudigel* [2004]

[a]NRM and fit directions are given as (declination, inclination).

temperatures close to the Curie temperature. As An-45 was heated in air, part of its magnetization decay during thermal demagnetization could be due to the reversal of iron and rutile to ilmenite.

5. Conclusion and Perspectives

We have designed and constructed an apparatus to conduct thermal demagnetization of extraterrestrial rocks under controlled atmosphere. A wide range of oxygen fugacities can be reached within the stability domain of iron, making it possible to conduct thermal demagnetization of extraterrestrial samples such as lunar rocks and meteorites. In particular, the intensity of the lunar dynamo is not well constrained: although it has been shown that the Moon had a stable magnetic field between at least 4.2 and 3.6 Ga [*Cournède et al*., 2012; *Garrick-Bethell et al*., 2009; *Shea et al*., 2012; *Suavet et al*., 2013], its intensity has been largely determined with AF methods, and therefore has an uncertainty factor of ∼3 due to the calibration between TRM and room temperature magnetizations (Tikoo et al., 2014). Thermal demagnetization of lunar and other extraterrestrial samples has the potential to provide paleointensity estimates with better accuracy, possibly comparable with that of typical terrestrial rocks (∼10% accuracy).

Acknowledgments

We thank J. Tyburczy and J. Feinberg for handling our manuscript, R. Harrison and an anonymous reviewer for their comments, B. Carbone for administrative support, and N. Chatterjee for help with the microprobe analyses. We thank the NASA Lunar Science Institute, the NASA Solar System Exploration and Research Virtual Institute, and the NASA Lunar Advanced Science and Exploration Research program. T.L.G. acknowledges support from NASA grant NNX12AH80G. The data for this paper are available at the Magnetics Information Consortium (MagIC) database.

References

Aitken, M. J., A. L. Allsop, G. D. Bussell, and M. B. Winter (1988), Determination of the intensity of the Earth's magnetic field during archaeological times: Reliability of the Thellier Technique, *Rev. Geophys.*, *26*, 3–12.

Bowles, J. A., L. Tatsumi-Petrochilos, J. E. Hammer, and S. A. Brachfeld (2012), Multicomponent cubic oxide exsolution in synthetic basalts: Temperature dependence and implications for magnetic properties, *J. Geophys. Res.*, *117*, B03202, doi:10.1029/2011JB008867.

Brecher, A., and L. Leung (1979), Ancient magnetic field estimates on selected chondritic meteorites, *Phys. Earth Planet. Inter.*, *20*, 361–378.

Brett, R., and M. Sato (1984), Intrinsic oxygen fugacity measurements on seven chondrites, a pallasite, and a tektite and the redox state of meteorite parent bodies, *Geochim. Cosmochim. Acta*, *48*, 111–120.

Burkhard, D. J. M., and G. C. Ulmer (1995), Kinetics and equilibria of redox systems at temperatures as low as 300°C, *Geochim. Cosmochim. Acta*, *59*, 1699–1714.

Cacciamani, G., J. De Keyzer, R. Ferro, U. E. Klotz, J. Lacaze, and P. Wollants (2006), Critical evaluation of the Fe–Ni, Fe–Ti, and Fe–Ni–Ti alloy systems, *Intermetallics*, *14*, 1312–1325.

Chowdhary, S. K., D. W. Collinson, A. Stephenson, and S. K. Runcorn (1987), Further investigations into lunar paleointensity determinations, *Phys. Earth Planet. Inter.*, *49*, 133–141.

Coe, R. S. (1967), The determination of paleo-intensities of the Earth's magnetic field with emphasis on mechanisms that could cause non-ideal behavior in Thellier's method, *J. Geomagn. Geolectr.*, *19*, 157–178.

Collinson, D. W. (1987), Magnetic properties of the Olivenza meteorite-possible implications for its evolution and an early solar system magnetic field, *Earth Planet. Sci. Lett.*, *84*, 369–380.

Collinson, D. W., A. Stephenson, and S. K. Runcorn (1973), Magnetic studies of Apollo 15 and 16 rocks, *Proc. Lunar Sci. Conf.*, *4th*, 3, 2963–2976.

Cournède, C., J. Gattacceca, and P. Rochette (2012), Magnetic study of large Apollo samples: Possible evidence for an ancient centered dipolar field on the Moon, *Earth Planet. Sci. Lett.*, *331–332*, 31–42.

Day, R., M. Fuller, and V. A. Schmidt (1977), Hysteresis properties of titanomagnetites: Grain-size and compositional dependence, *Phys. Earth Planet. Inter.*, *13*, 260–267.

Dunlop, D. J., and O. Özdemir (1997), *Rock Magnetism: Fundamentals and Frontiers*, 573 pp., Cambridge Univ. Press, New York, N. Y.

Dunn, J. R., and M. Fuller (1972), Thermoremanent magnetization (TRM) of lunar samples, *Moon*, *4*, 49–62.

Eugster, H. P., and D. R. Wones (1962), Stability relations of the Ferruginous Biotite, Annite, *J. Petrol.*, *3*(1), 82–125.

Fuller, M., and S. M. Cisowski (1987), Lunar paleomagnetism, in *Geomagnetism*, edited by J. A. Jacobs, pp. 307–455, Academic, Orlando, Fla.

Fuller, M., E. Meshkov, and C. S. Cisowski (1979), On the natural remanent magnetism of certain mare basalts, *Proc. Lunar Planet. Sci. Conf.*, *10th*, 3, 2211–2233.

Garrick-Bethell, I., and B. P. Weiss (2010), Kamacite blocking temperatures and applications to lunar magnetism, *Earth Planet. Sci. Lett.*, *294*, 1–7.

Garrick-Bethell, I., B. P. Weiss, D. L. Shuster, and J. Buz (2009), Early lunar magnetism, *Science*, *323*, 356–359.

Gattacceca, J., and P. Rochette (2004), Toward a robust normalized magnetic paleointensity method applied to meteorites, *Earth Planet. Sci. Lett.*, *227*, 377–393.

Goodrich, C. A., S. R. Sutton, S. Wirick, and M. J. Jercinovic (2013), Chromium valences in ureilite olivine and implications for ureilite petrogenesis, *Geochim. Cosmochim. Acta*, *122*, 280–305.

Gose, W. A., D. W. Strangway, and G. W. Pearce (1973), A determination of the intensity of the ancient lunar magnetic field, *Moon*, *7*, 196–201.

Grove, T. L., and D. W. Beaty (1980), Classification, experimental petrology and possible volcanic histories of the Apollo 11 high-K basalts, *Proc. Lunar Planet. Sci. Conf.*, *11th*, 1, 149–177.

Halgedahl, S. L., S. R. Day, and M. Fuller (1980), The effect of cooling rate on the intensity of weak-field TRM in single-domain magnetite, *J. Geophys. Res.*, *95*, 3690–3698.

Hewins, R. H., and G. C. Ulmer (1984), Intrinsic oxygen fugacities of diogenites and mesosiderite clasts, *Geochim. Cosmochim. Acta*, *48*, 1555–1560.

Hoffman, K. A., J. R. Baker, and S. K. Banerjee (1979), Combining paleointensity methods: A dual-valued determination on lunar sample 10017,135, *Phys. Earth Planet. Inter.*, *20*, 317–323.

Huebner, J. S. (1975), Oxygen fugacity values of furnace gas mixtures, *Am. Mineral.*, *60*, 815–823.

Keller, L., M. Loeffler, R. Christoffersen, C. Dukes, Z. Rahman, and R. Baragiola (2010), Irradiation of FeS; implications for the lifecycle of sulfur in the interstellar medium and presolar FeS grains, in *Abstracts of Papers Submitted to the Lunar and Planetary Science Conference*, *Forty-First Lunar and Planetary Science Conference XLI*, vol. 41, pp. 1172, Houston, Tex.

Kirschvink, J. L. (1980), The least-squares line and plane and the analysis of paleomagnetic data: Examples from Siberia and Morocco, *Geophys. J. R. Astron. Soc.*, *62*, 699–718.
Kletetschka, G., M. H. Acuna, T. Kohout, P. J. Wasilewski, and J. E. P. Connerney (2004), An empirical scaling law for acquisition of thermoremanent magnetization, *Earth Planet. Sci. Lett.*, *226*, 521–528.
Larson, E. E. (1978), Degradation of lunar basalts during thermal heating in vacuum and its relation to paleointensity measurements, in *Lunar and Planetary Science IX*, edited, p. 633, Lunar and Planet. Inst., Houston, Tex.
Larson, E. E., R. P. Hoblitt and D. E. Watson (1975), Gas-mixing techniques in thermomagnetic analysis, *Geophys. J. R. Astron. Soc.*, *43*(2), 607–620.
Lawrence, K., C. Johnson, L. Tauxe, and J. Gee (2008), Lunar paleointensity measurements: Implications for lunar magnetic evolution, *Phys. Earth Planet. Inter.*, *168*, 71–87, doi:10.1016/j.pepi.2008.05.1007.
Levi, S. (1977), The effect of magnetite particle size on paleointensity determinations of the geomagnetic field, *Phys. Earth Planet. Inter.*, *13*, 245–259.
Morden, S. J. (1992), A magnetic study of the Millbillillie (eucrite) achondrite: Evidence for dynamo-type magnetising field, *Meteoritics*, *27*, 560–567.
Nafziger, R., G. Ulmer, and E. Woermann (1971), Gaseous buffering for the control of oxygen fugacity at one atmosphere, in *Research Techniques for High Pressure and High Temperature*, edited by G. Ulmer, pp. 9–41, Springer, Berlin.
Nagata, T. (1961), *Rock Magnetism*, 350 pp., Maruzen Co., Tokyo.
Néel, L. (1949), Théorie du trainage magnétique des ferromagnétiques en grains fins avec applications aux terres cuites, *Ann. Geofis.*, *5*, 99–136.
Pearce, G. W., G. S. Hoye, D. W. Strangway, B. M. Walker, and L. A. Taylor (1976), Some complexities in the determination of lunar paleointensities, *Proc. Lunar Sci. Conf.*, *7th*, 3, 3271–3297.
Prunier, A. R., and D. A. Hewitt (1981), Calculation of temperature-oxygen fugacity tables for H2-Co2 gas-mixtures at one atmosphere total pressure—Summary, *Geol. Soc. Am. Bull.*, *92*(7), 414–416.
Righter, K., and K. E. Neff (2007), Temperature and oxygen fugacity constraints on CK and R chondrites and implications for water and oxidation in the early solar system, *Polar Sci.*, *1*(1), 25–44.
Sato, M. (1971), Electrochemical measurements and control of oxygen fugacity and other gaseous fugacities with solid electrolyte sensors, in *Research Techniques for High Pressure and High Temperature*, edited by G. C. Ulmer, pp. 43–99, Springer, Berlin.
Sato, M., N. L. Hickling, and J. E. McLane (1973), Oxygen fugacity values of Apollo 12, 14, and 15 lunar samples and reduced state of lunar magmas, in *Proc. Lunar Sci. Conf., 4th*, *1*, 1061–1079.
Shaar, R., and L. Tauxe (2013), Thellier GUI: An integrated tool for analyzing paleointensity data from Thellier-type experiments, *Geochem. Geophys. Geosyst.*, *14*(3), 677–692.
Shea, E. K., B. P. Weiss, W. S. Cassata, D. L. Shuster, S. M. Tikoo, J. Gattacceca, T. L. Grove, and M. D. Fuller (2012), A long-lived lunar core dynamo, *Science*, *335*, 453–457.
Suavet, C., B. P. Weiss, W. S. Cassata, D. L. Shuster, J. Gattacceca, L. Chan, I. Garrick-Bethell, J. W. Head, T. L. Grove, and M. D. Fuller (2013), Persistence and origin of the lunar core dynamo, *Proc. Natl. Acad. Sci. U. S. A.*, *110*, 8453–8458.
Sugiura, N., and D. W. Strangway (1980), Comparisons of magnetic paleointensity methods using a lunar sample, *Proc. Lunar Planet. Sci. Conf.*, *11th, 3*, 1801–1813.
Sugiura, N., and D. W. Strangway (1983), Magnetic paleointensity determination on lunar sample 62235, *Proc. Lunar Planet. Sci. Conf. 13th*, Part 2, *J. Geophys. Res.*, *88*, suppl., A684-A690.
Sugiura, N., D. W. Strangway, and G. W. Pearce (1978), Heating experiments and paleointensity determinations, *Proc. Lunar Planet. Sci. Conf.*, *9th*, 3, 3151–3163.
Sugiura, N., Y. M. Wu, D. W. Strangway, G. W. Pearce, and L. A. Taylor (1979), A new magnetic paleointensity value for a "young lunar glass", *Proc. Lunar Planet. Sci. Conf.*, *10th*, 3, 2189–2197.
Tauxe, L. (2010), *Essentials of Paleomagnetism*, 512 pp., Univ. of Calif. Press, Berkeley., Calif.
Tauxe, L., and H. Staudigel (2004), Strength of the geomagnetic field in the Cretaceous Normal Superchron: New data from submarine basaltic glass of the Troodos Ophiolite, *Geochem. Geophys. Geosyst.*, *5*, Q02H06, doi:10.1029/2003GC000635.
Taylor, L. A. (1979), Paleointensity determinations at elevated temperatures: Sample preparation technique, *Proc. Lunar Planet. Sci. Conf.*, *10th*, 3, 2183–2187.
Taylor, L. A., R. J. Williams, and R. H. McCallister (1972), Stability relations of ilmenite and ulvöspinel in the Fe-Ti-O system and application of these data to lunar mineral assemblages, *Earth Planet. Sci. Lett.*, *16*, 282–288.
Thellier, E., and O. Thellier (1959), Sur l'intensité du champ magnétique terrestre dans le passé historique et géologique, *Ann. Geofis.*, *15*, 285–376.
Tikoo, S. M., B. P. Weiss, W. S. Cassata, D. L. Shuster, J. Gattacceca, E. A. Lima, C. Suavet, F. Nimmo, and M. D. Fuller, (2014), Decline of the lunar core dynamo, *Earth Planet. Sci. Lett.*, in press.
Ulmer, G., and E. Woermann (2007), Thermodynamic price tags for a wet mantle, *Geochim. Cosmochim. Acta*, *71*(15), supplement, 1046.
Wadhwa, M. (2008), Redox conditions on small bodies, the Moon and Mars, *Rev. Mineral. Geochem.*, *68*, 493–510.
Wang, H., and D. V. Kent (2013), A paleointensity technique for multidomain igneous rocks, *Geochem. Geophys. Geosyst.*, *14*, 4195–4213, doi:10.1002/ggge.20248.
Watson, D. E., E. E. Larson, and R. L. Reynolds (1974), Microscopic and thermomagnetic analysis of Apollo 17 breccia and basalt: Feasibility of obtaining meaningful paleointensities of the lunar magnetic field, in *Lunar and Planetary Science V*, edited, pp. 827–829, Lunar and Planet. Inst., Houston, Tex.
Weiss, B. P., J. Gattacceca, S. Stanley, P. Rochette, and U. R. Christensen (2010), Paleomagnetic records of meteorites and early planetesimal differentiation, *Space Sci. Rev.*, *152*, 341–390.
Westphal, M. (1986), Natural remanent magnetization, thermoremanent magnetization and reliability of paleointensity determinations on H chondrites, *Phys. Earth Planet. Inter.*, *43*, 300–306.
Westphal, M., and H. Whitechurch (1983), Magnetic properties and paleointensity determination of seven H-group chondrites, *Phys. Earth Planet. Inter.*, *31*, 1–9.
Yu, Y. (2010), Paleointensity determination using anhysteretic remanence and saturation isothermal remanence, *Geochem. Geophys. Geosyst.*, *11*, Q02Z12, doi:10.1029/2009GC002804.
Yu, Y., L. Tauxe, and A. Genevey (2004), Toward an optimal geomagnetic field intensity determination technique, *Geochem. Geophys. Geosyst.*, *5*, Q02H07, doi:10.1029/2003GC000630.
Yu, Y. J. (2006), How accurately can NRM/SIRM determine the ancient planetary magnetic field intensity?, *Earth Planet. Sci. Lett.*, *250*, 27–37.
Zen, E.-A. (1985), An oxygen buffer for some peraluminous granites and metamorphic rocks, *Am. Mineral.*, *70*, 65–73.